NANO · MICRO small

Supporting Information

for *Small*, DOI 10.1002/smll.202309906

An Active and Robust Catalytic Architecture of NiCo/GaN Nanowires for Light-Driven Hydrogen Production from Methanol

Jinglin Li, Bowen Sheng, Yiqing Chen, Jiajia Yang, Ping Wang, Yixin Li, Tianqi Yu, Hu Pan, Jun Song, Lei Zhu, Xinqiang Wang*, Tao Ma and Baowen Zhou**

An Active and Robust Catalytic Architecture of NiCo/GaN NWs for Light-Driven Hydrogen Production from Methanol

Jinglin Li[1+], Bowen Sheng[2+], Yiqing Chen[3+], Jiajia Yang[2], Ping Wang[2], Yixin Li[1], Tianqi Yu[1], Hu Pan[1], Jun Song[3]*, Lei Zhu[1], Xinqiang Wang[2,4,5]*, Tao Ma[6], Baowen Zhou[1]*.

1. Key Laboratory for Power Machinery and Engineering of Ministry of Education, Research Center for Renewable Synthetic Fuel, School of Mechanical Engineering, Shanghai Jiao Tong University, 800 Dongchuan Road, Shanghai 200240, China.
2. State Key Laboratory of Artificial Microstructure and Mesoscopic Physics, School of Physics, Nano-Optoelectronics Frontier Center of Ministry of Education (NFC-MOE), Peking University, Beijing 10087, China.
3. Department of Mining and Materials Engineering, McGill University, 3610 University Street, Montreal, QC H3A0C9, Canada
4. Peking University Yangtze Delta Institute of Optoelectronics, Nantong, Jiangsu 226010, China
5. Collaborative Innovation Center of Quantum Matter, School of Physics, Peking University, Beijing 100871, China.
6. Michigan Center for Materials Characterization $(MC)^2$, University of Michigan, Ann Arbor, MI 48109, USA.

* Corresponding authors Email: jun.song2@mcgill.ca; wangshi@pku.edu.cn; zhoubw@sjtu.edu.cn

+ These authors contributed equally to this work.

Methods

MBE growth of the semiconducting support platform. Catalyst-free GaN NWs were grown on a 4-inch Si (111) wafer by a plasma-assisted SVTA MBE system under nitrogen-rich conditions. First, the standard pre-growth processes including high-temperature degas and nitridation was performed. Then, the nanowire growth was carried out maintaining a constant nitrogen flux and growth temperature of 700 ℃. The nanowire consists of approximately 400 nm unintendedly doped GaN and a 300 nm p-

GaN layer. The p-GaN layer with Mg doping was grown by ladder Mg cell temperatures in the order of 230 ℃, 250 ℃, and 270 ℃. To be noted, the nanowires have been formed during a continuous growth process by only switching on Mg flux without any growth interruption.

The immobilization of NiCo species. The immobilization of NiCo was carried out in a sealed Pyrex chamber with a quartz lid via a photo-deposition process. GaN NWs supported by silicon wafer, methanol aqueous solution with a volume MeOH/H_2O ratio of 1/5, and a certain amount of Ni and Co precursors ($NiCl_2$, $CoCl_2$, Shanghai Aladdin Biochemical Technology Co., Ltd.) were added into the chamber. The chamber was then vacuumed and filled with Ar, followed by light irradiation with a 300 Xe lamp for 30 min to immobilize NiCo nanoclusters on the surface of GaN NWs. The assembled architecture is denoted as NiCo/GaN NWs. Ni/GaN NWs and Co/GaN NWs were prepared by the identical procedure for comparison, and the major difference is the precursors utilized for photo-deposition.

Characterization. The X-ray diffraction (XRD) patterns of the samples were measured by a Bruker D8 Advance diffractometer (with Cu Kα, at 60 kV and 80 mA). X-ray photoelectron spectroscopy (XPS) was characterized by an ESCALAB 250xi non-monochromatic Al anodes, and the binding energy was corrected by using C 1s peak at 284.8 eV as the internal standard. ICP-OES measurements were performed to estimate the accurate loaded amount of NiCo nanoclusters using an AGILENT ICP-OES 730. PL and TR-PL spectroscopies were characterized by an FLS980 (Edinburgh Instruments). TGA was measured using an STA 449 F3 Jupiter in the air. Scanning electron microscopy (SEM) images were obtained using a Quattro ESEM (Thermo Fisher). High-angle annular dark field-scanning transmission electron microscopy (HAADF-STEM) images were captured by a Thermo Fisher Scientific Talos F200X S/TEM, equipped with a Super-X EDS detector and operated at 200 kV. Transmission electron microscopy (TEM) images were obtained using a JEOL 2100F microscope. *Operando* DRIFT characterization was carried out by Frontier FT-IR Spectrometer, PerkinElmer, which was equipped with an MCT detector and 10-cm Demountable Gas Cell. In the process of DRFTI measurement, the photocatalyst was fixed at the bottom of the Gas Cell. Subsequently, the reaction gas was injected into the Gas Cell by a

bubbling system. After reaching the adsorption-desorption equilibrium between the reaction gas and the sample, the background spectrum of the system was recorded. Then, the injection of the reaction gas was stopped and the Gas Cell was closed, and the light intensity of 4 $W \cdot cm^{-2}$ was applied from the top of the Gas Cell. The data were recorded every 3 minutes. *In situ* EPR characterization was conducted on a Bruker A300 (Germany) and DMPO was used as a spin trap.

Performance evaluation. In the lab, light-driven hydrogen production from methanol was conducted in a 0.44 L home-made sealed Pyrex chamber equipped with a quartz lid. Before being fixed at the bottom of the Pyrex chamber, the catalysts of NiCo-decorated GaN NWs supported by Si wafer (~0.5 cm^{-2}, ~0.34 mg cm^{-2}) were thoroughly washed with deionized water. After evacuation, the chamber was filled with Ar until atmospheric pressure. Subsequently, 1 mL methanol (AR, 99.5%, Chemical Reagent Co., Ltd.) was injected into the chamber. Photocatalytic reactions were carried out under illumination by a 300 W Xenon lamp with full spectrum at 5 W cm^{-2} for 15 min if not specifically noted. The optical intensity can be easily modulated by changing the current of the setup. The surface temperature of the catalyst was recorded by an infrared thermography (FOTRFIC 315, Shanghai Thermal Imaging Technology Co., Ltd.). The thermocatalytic experiments were performed using a high temperature electric tube furnace with a 0.25 L stainless-steel pipe without illumination. The outdoor test was carried out by a customer-built device as shown in **Fig. 2E**. The catalyst wafer was installed into a well-designed chamber, which was stabilized on a support frame. The Fresnel lens was used to generate concentrated sunlight on the plane region where the catalyst wafer was stabilized, and the light intensity was varied from 1 $W \cdot cm^{-2}$ to 9 $W \cdot cm^{-2}$, which was associated with the testing time and weather conditions. A photosensitive detector was used to adjust the angle of the Fresnel lens to illuminate the catalyst with the maximum light intensity. In the outdoor test, the chamber was vacuumed and filled with argon every hour to exclude the produced hydrogen prior to the next circle. Meanwhile, thermo-catalytic reactions were conducted in a tubular furnace equipped with NiCo/GaN NWs under 1 atm argon atmosphere.

The gaseous products were analyzed by a gas chromatograph (GC-9080, Sun) equipped with a flame ionization detector (FID) detector and a thermal conductivity detector (TCD), respectively. Calculations of H_2 evolution rate, turnover frequency (TOF), and turnover number (TON) were conducted based on the following equations:

$$H_2 \text{ evolution rate} = \frac{H_2 \text{ yield per unit area of catalyst per hour}}{\text{Mass of catalyst per unit area}} \quad \textbf{(S1)}$$

$$\text{Mass of catalyst per unit area} = L \times \nu \times 6.1 \text{ g·cm}^{-3} \times 1 \text{ cm}^{-2} \quad \textbf{(S2)}$$

Where the L is the length of GaN NWs, which was estimated at about 900 nm, and the ν was denoted as the fill factor, which was estimated to be approximately 62.2% according to the top-view SEM image of GaN NWs on Si substrate (**Fig. S3**). Considering that the density of GaN is 6.1 g·cm^{-3}, the deposited amount of photocatalysts onto silicon substrate is calculated to be about 0.34 mg·cm^{-2}. Due to the low content (<0.01 mg), the cocatalyst of Ni and Co was not taken into consideration.

$$\text{TOF} = \frac{H_2 \text{ evolution rate}}{\text{Content of immobilized NiCo nanoclusters}} \quad \textbf{(S3)}$$

$$\text{TON} = \frac{\text{Yield of } H_2}{\text{Content of immobilized NiCo nanoclusters}} \times 100\% \quad \textbf{(S4)}$$

The AQE (φ) was calculated by this equation:

$$\varphi = \frac{nR}{I} \quad \textbf{(S5)}$$

where the n is the number of involved electrons, the R is hydrogen evolution rate (**Fig. S13A**), and the I is the amount of incident protons.[1-2] The monochromatic light was equipped with a quartz lens, and the light intensities (P) at wavelengths of 275, 420, 535, and 730 nm are 36.7, 551.0, 167.3, and 312.2 mW·cm^{-2}, respectively. For all measurements, the light irradiation area (S) is 0.65 cm^{-2}, which is the area of the photocatalyst. The reaction temperature was controlled at 220 ℃ by a heating platform for quick observation of the results. The irradiation time (T) of the monochromatic light was 3600 s. The detailed calculation is shown below.[1-2]

$$I = \frac{E\lambda}{hc} \times S = \frac{PT\lambda}{hc} \times S \quad \textbf{(S6)}$$

Where E is the energy of photons, λ is the wavelength of monochromatic light, h is the Plank constant, and c is the speed of light.

Computational methods. Spin-polarized density function theory (DFT) calculations were performed employing the Vienna Ab Initio Simulation Package (VASP).[3-4] The interaction between valence electrons and ions were described by the projector-augmented wave (PAW) method.[5] The exchange correlation of the Kohn-Sham equation was presented by generalized gradient approximation (GGA) with the Perdew-Burke-Ernzerhof (PBE) functional.[6-7] For calculations related to adsorption, van der Waals (vdW) interactions were included using Grimme's DFT-D3 method.[8-9] A plane-wave basic set was used to expand the wavefunctions with the kinetic cutoff energy set to 500 eV. For the calculations of slabs, a 2 × 2 × 1 Mokhorst-Pack k-point grid was implemented to sample the Brillouin zone.[10] During the geometry optimization, the convergence criteria for the atomic forces and the total energies were set to 0.02 eV/Å and 10^{-5} eV, respectively.

As the m-plane of GaN was observed in experiments, we constructed GaN $(10\bar{1}0)$ surface with a 4 × 2 supercell containing 6 layers to represent the pristine GaN. Besides, Ni/GaN and NiCo/GaN were created by depositing a small cluster of metal atoms on GaN $(10\bar{1}0)$. The top and side views of optimized geometries of GaN $(10\bar{1}0)$, Ni/GaN, and NiCo/GaN are represented in **Fig. S17**. To avoid image interaction, a vacuum spacing of at least 12 Å was set along the normal direction to the surface for all slab models and along all three directions for nanoparticles. Moreover, for all slab models, the bottom three layers of GaN were fixed in their bulk positions during structural relaxation.

The free energies of methanol reforming were calculated based on the computational hydrogen electrode (CHE) model.[11] The Gibbs free energy of adsorption ΔG was calculated via the:

$$\Delta G = E_{ad} + \Delta ZPE - T\Delta S \quad \textbf{(S7)}$$

where E_{ad} is the adsorption energy defined by:

$$E_{ad} = E_{surface+adsorbate} - E_{surface} - E_{adsorbate} \quad \textbf{(S8)}$$

ΔZPE and ΔS are the changes in zero-point energy and entropy during adsorption.

Table S1 | Catalytic activity of various catalysts for MeOH reforming to hydrogen in recent years.

Catalysts	Light source	Activity ($mol \cdot g_{cat}^{-1} \cdot h^{-1}$)	TOF (h^{-1})	Durability (h)	TON	Ref.
NiCo/GaN NWs	300 W Xe lamp	5.62	46460	600	1.6×10^7	This work
ZnCu Alloy	AM 1.5G	0.328	-	4	-	[2]
Pt/CN	450 W Xe lamp	3.3	-	38	4.7×10^5	[12]
NiO_x/TiO_2	300 W Xe lamp	0.032	-	30	-	[13]
$Sr_2MgSi_2O_7:Eu^{2+}$, Dy^{3+}	500 W mercury lamp	0.014	-	10	-	[14]

Table S2. The measured amounts of cocatalysts of Ni and Fe in the optimized NiFe NPs/GaN NWs/Si.

Ni ($\mu mol \cdot cm^{-2}$)	Co ($\mu mol \cdot cm^{-2}$)	Total ($\mu mol \cdot cm^{-2}$)
0.0212	0.228	0.44

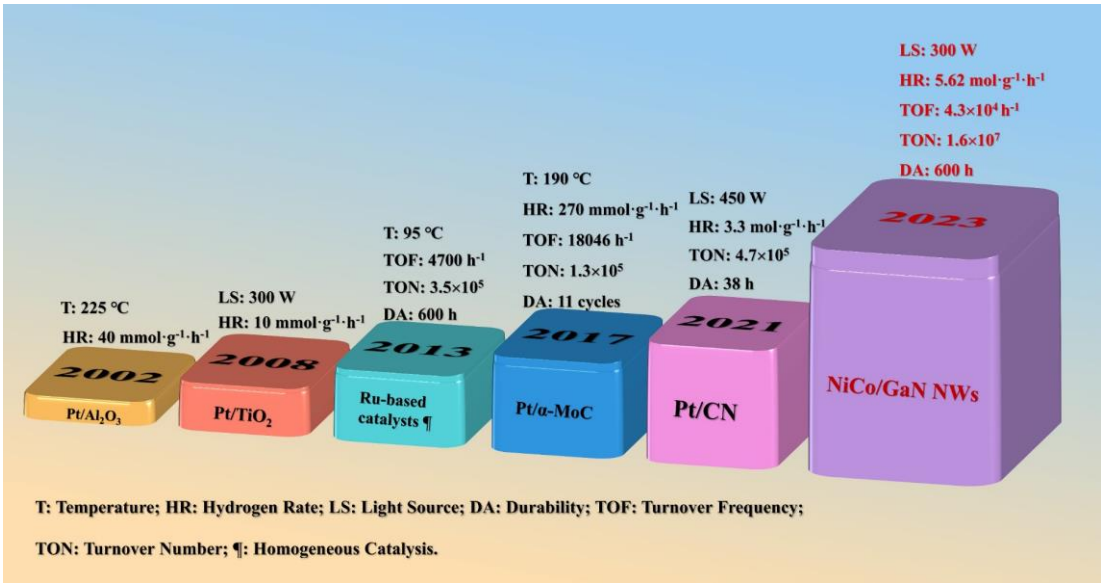


Fig. S1. Benchmarking progress of on-site hydrogen production from methanol by various approaches including photocatalysis and thermo-catalysis.

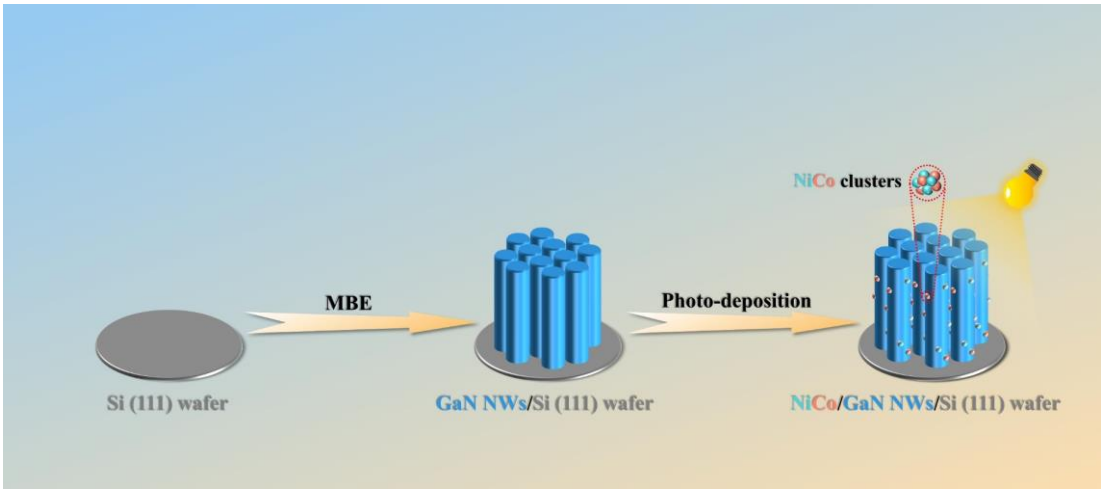


Fig. S2. Schematic diagram for the decoration of NiCo nanoclusters onto GaN NWs by combining plasma-assisted MBE with photo-deposition.

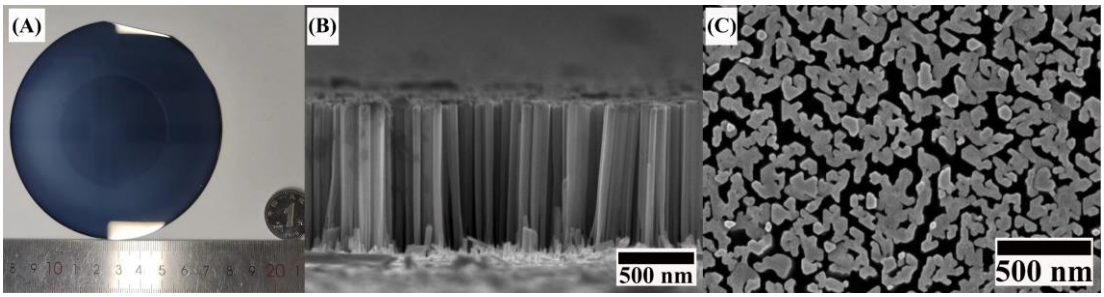


Fig. S3. The digital photo (A) and SEM images of GaN NWs/Si vertically assigned onto Si wafer. (B) Side view. (C) Top view.

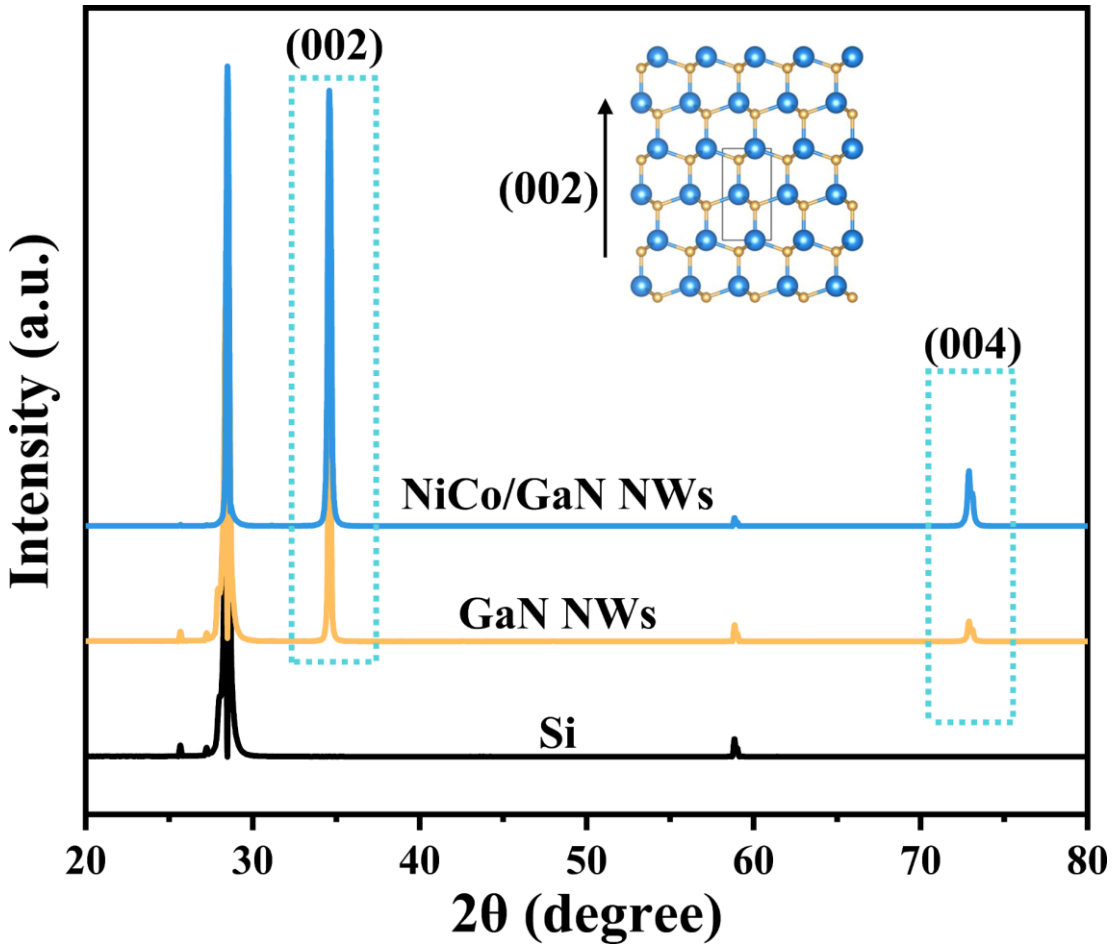


Fig. S4. XRD patterns of Si wafer, GaN NWs/Si, and NiCo/GaN NWs supported by Si wafer, respectively.

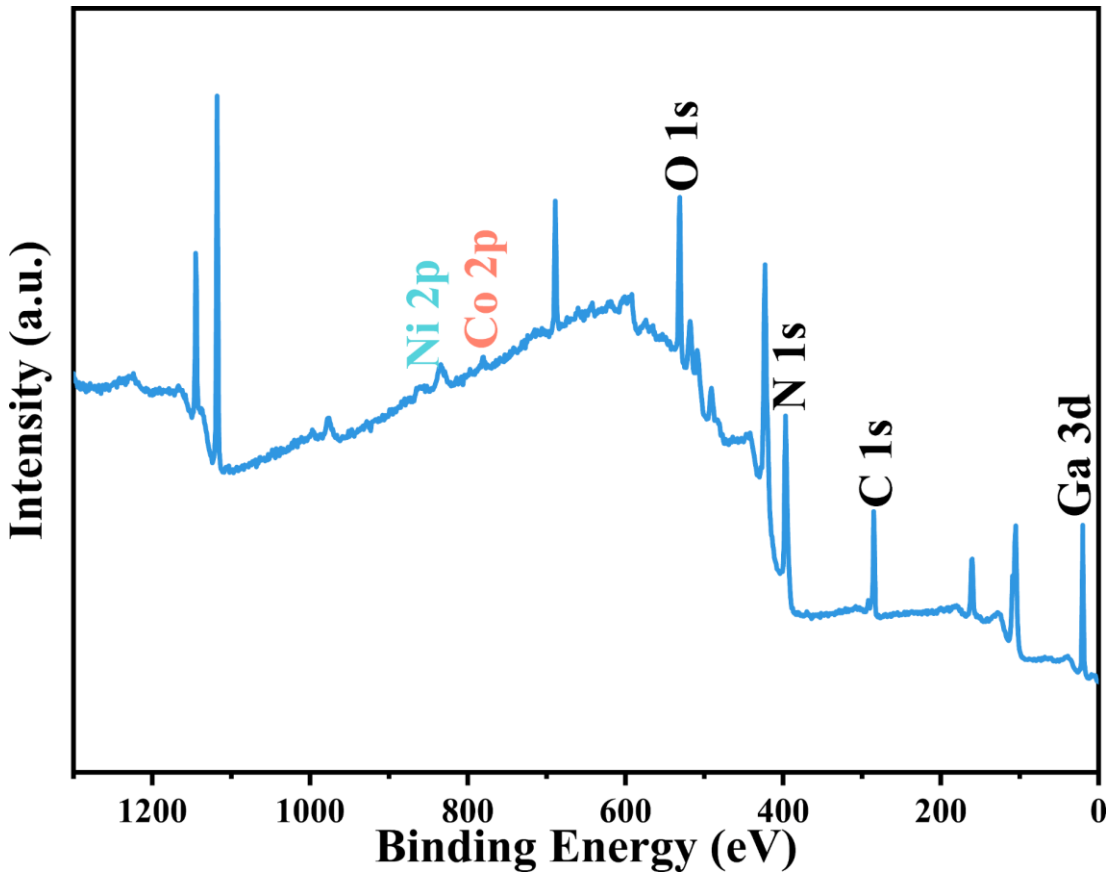


Fig. S5. XPS survey of NiCo/GaN NWs supported by Si substrate.

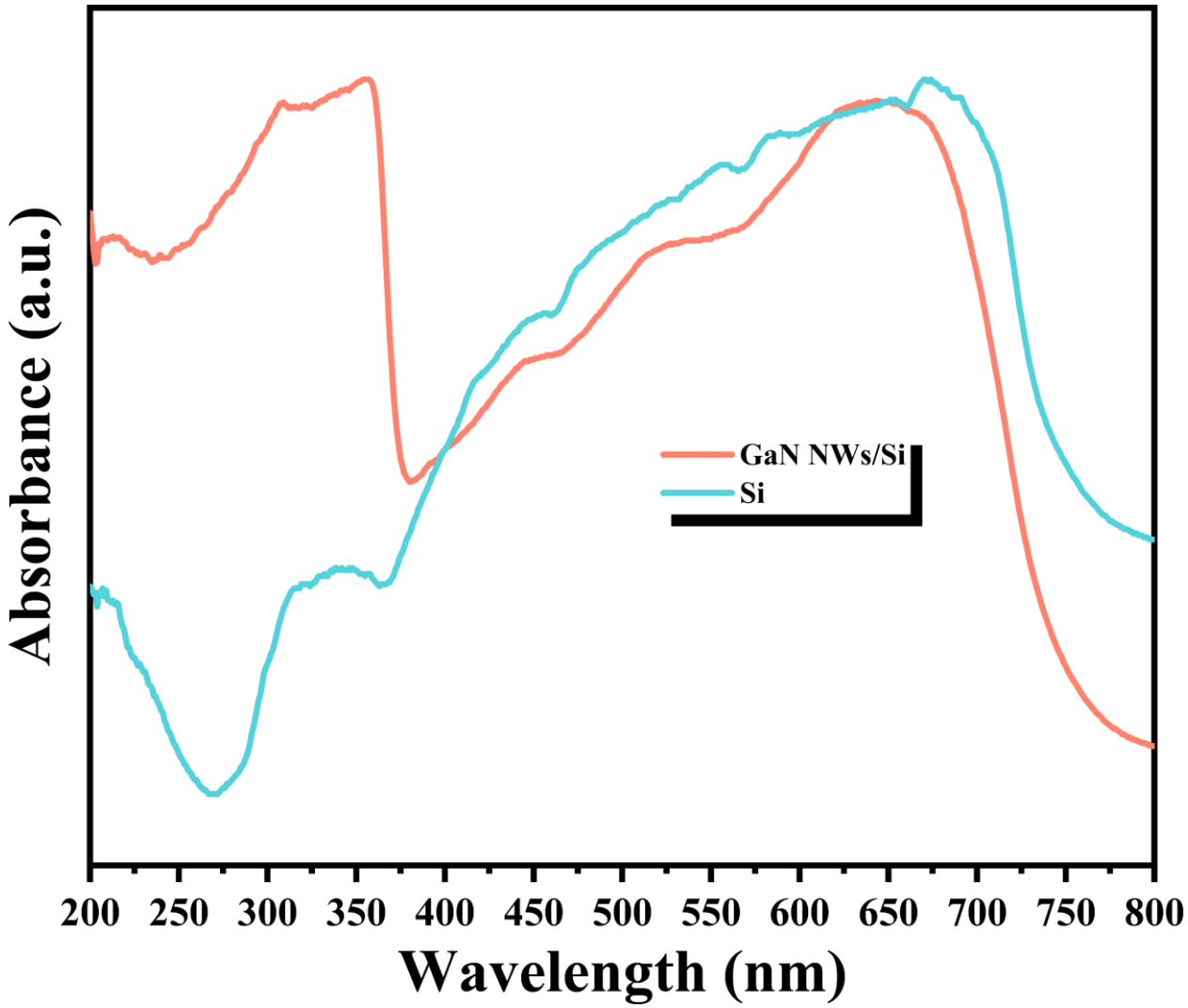


Fig. S6. UV-vis absorption spectra of GaN NWs/Si and Si.

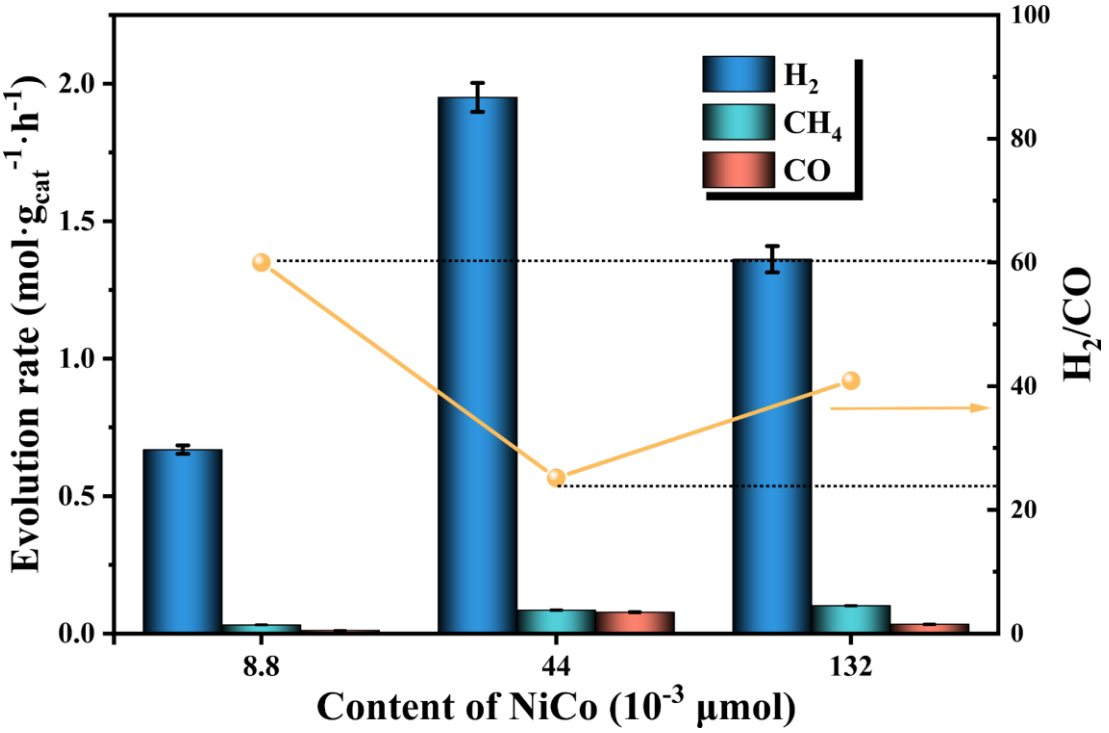


Fig. S7. Influence of content of NiCo on H_2 evolution rate over NiCo- decorated GaN NWs. The error bars are 2.3%s.e.m. for the content of 8.8 μmol, 2.7%s.e.m. for the content of 44 μmol, and 3.5%s.e.m. for the content of 132 μmol.

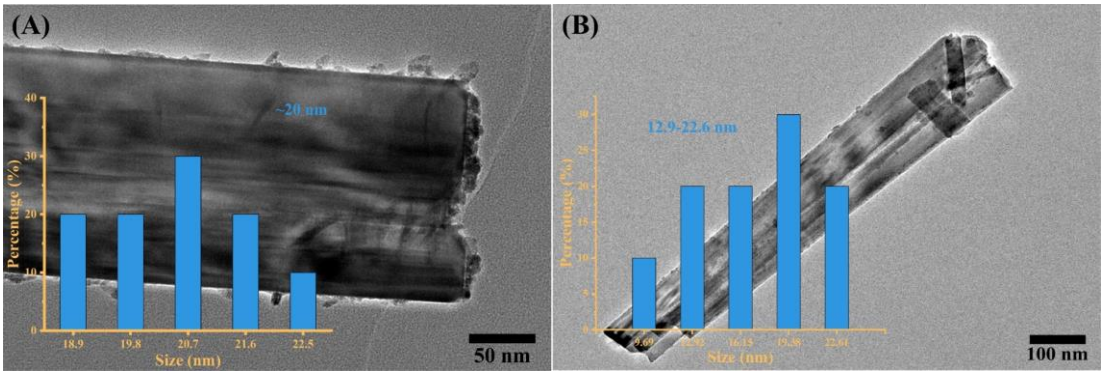


Fig. S8. TEM images and diameters distribution (inset) of different amounts of NiCo supported by GaN NWs with (A) 0.044 and (B) 0.132 μmol·cm^{-2}.

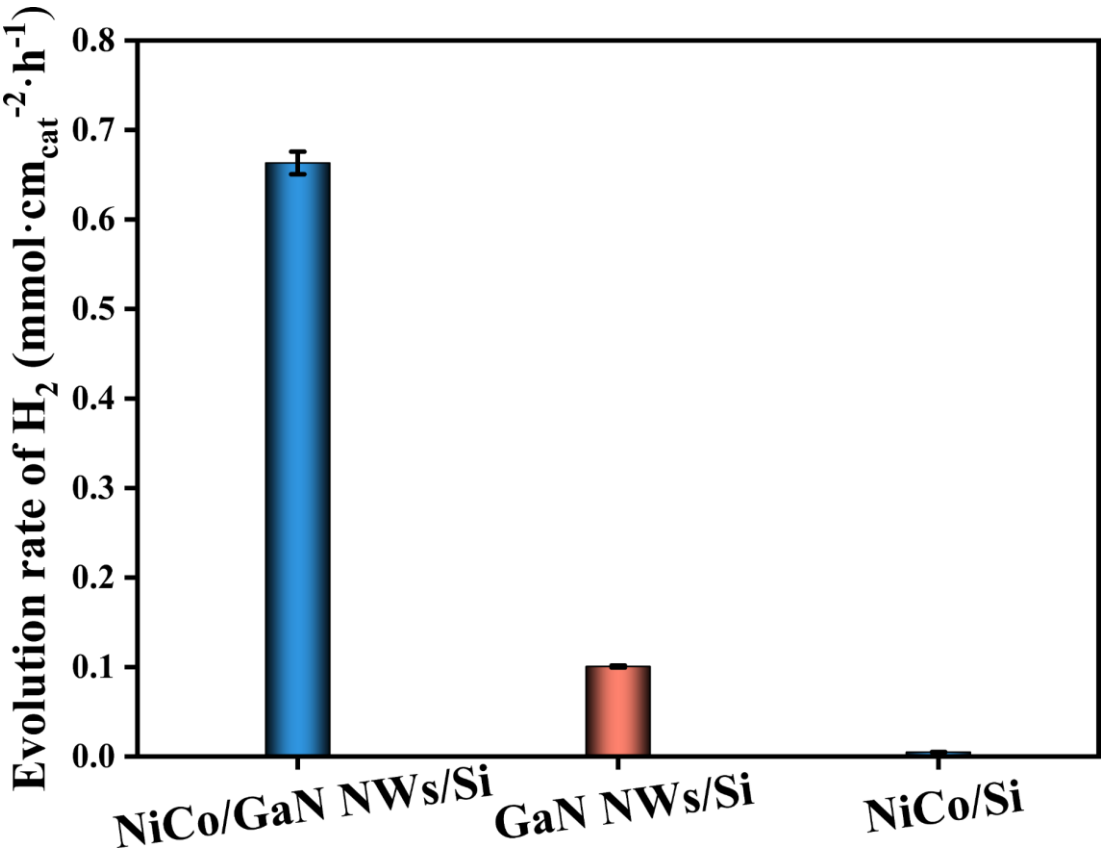


Fig. S9. The area activity of H_2 over NiCo/GaN NWs/Si, GaN NWs/Si, and Si. The error bars are 0.66 ± 2.7%s.e.m. for NiCo/GaN NWs, 0.10 ± 1.1%s.e.m., and 0.0049 ± 0.21%s.e.m for NiCo/Si.

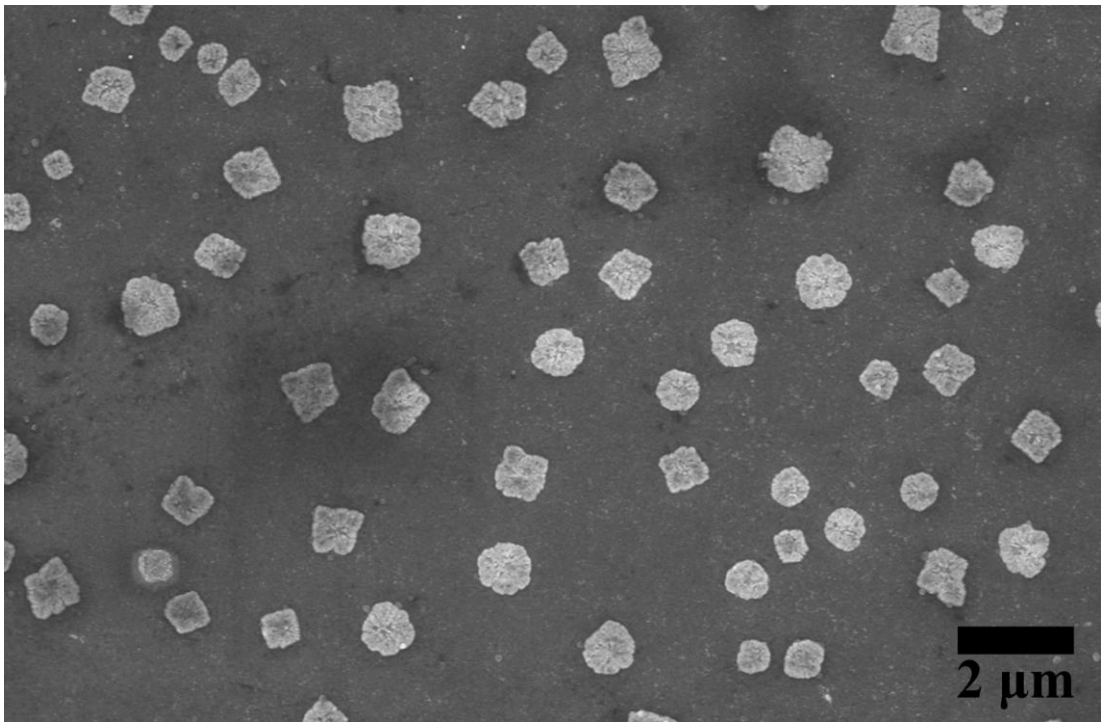


Fig. S10. SEM image of NiCo/Si.

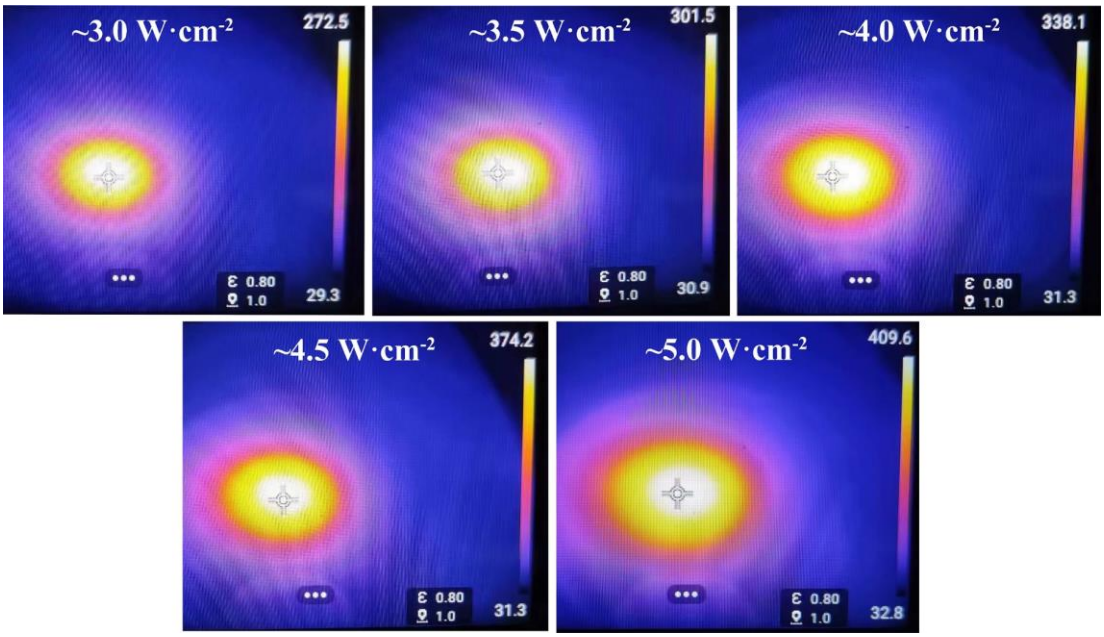


Fig. S11. Infrared thermal images of NiCo/GaN NWs under various light intensities.

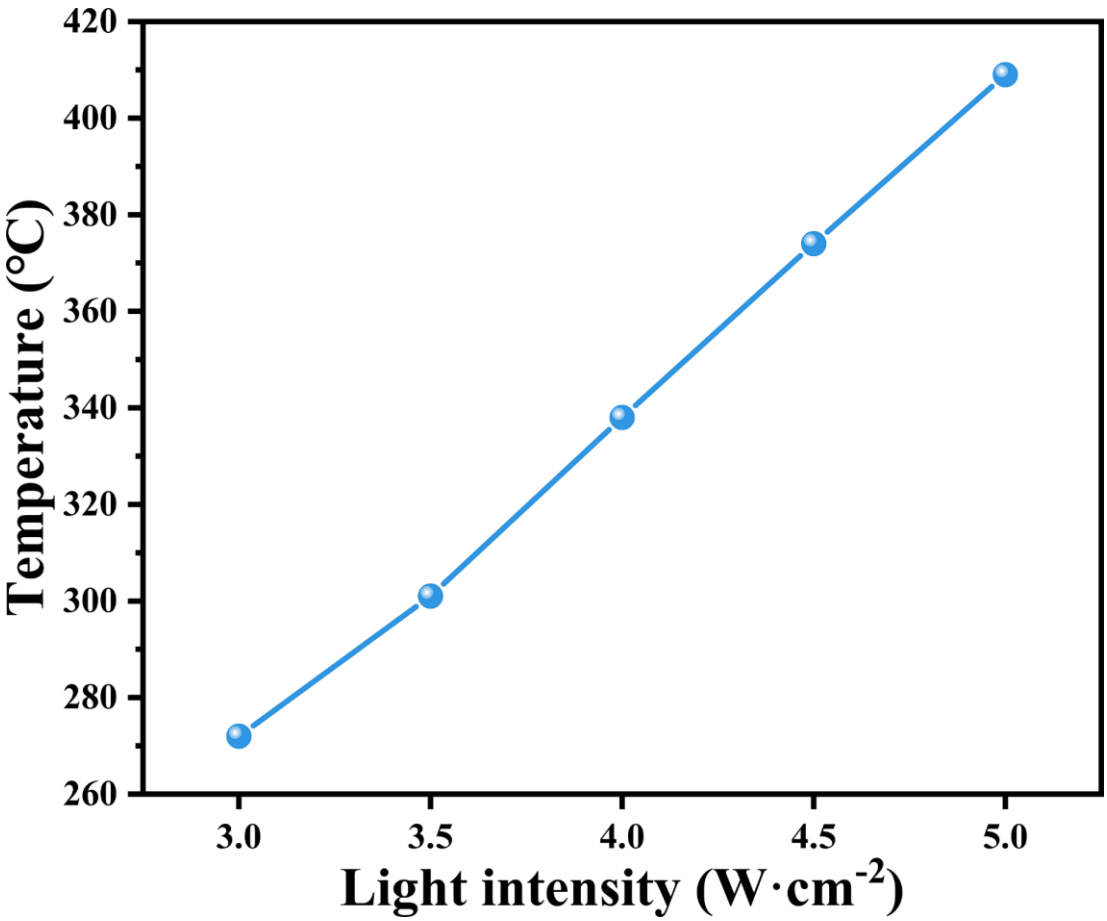


Fig. S12. Surface temperature curves of NiCo/GaN NWs under various light intensities.

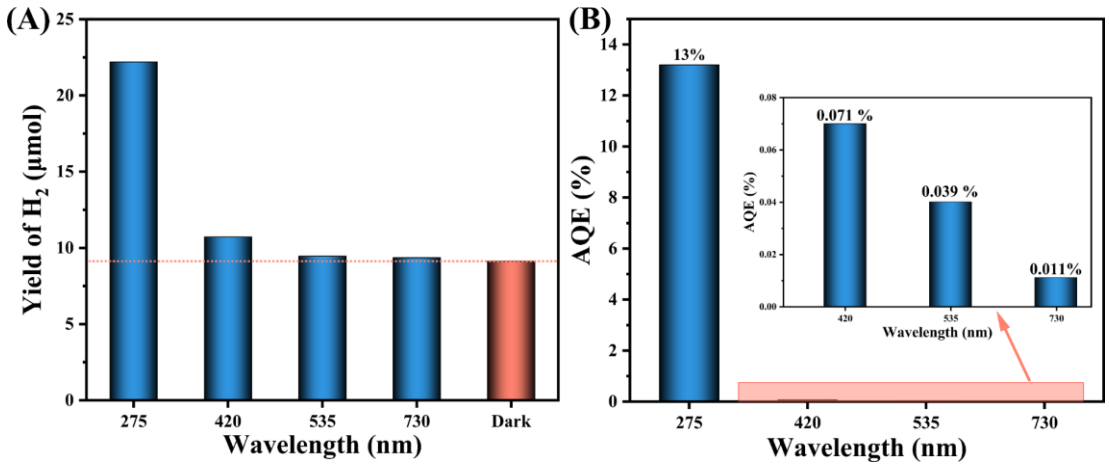


Fig. S13. (A) The yield of H_2 over NiCo/GaN NWs/Si under different monochromatic light and dark conditions at 220 ℃ in the reactor (260 mL). The mass of the photocatalyst was calculated to be 0.221 mg. (B) The apparent quantum efficiency values of NiCo/GaN NWs/Si at 220 °C with monochromatic light irradiation in different wavelengths.

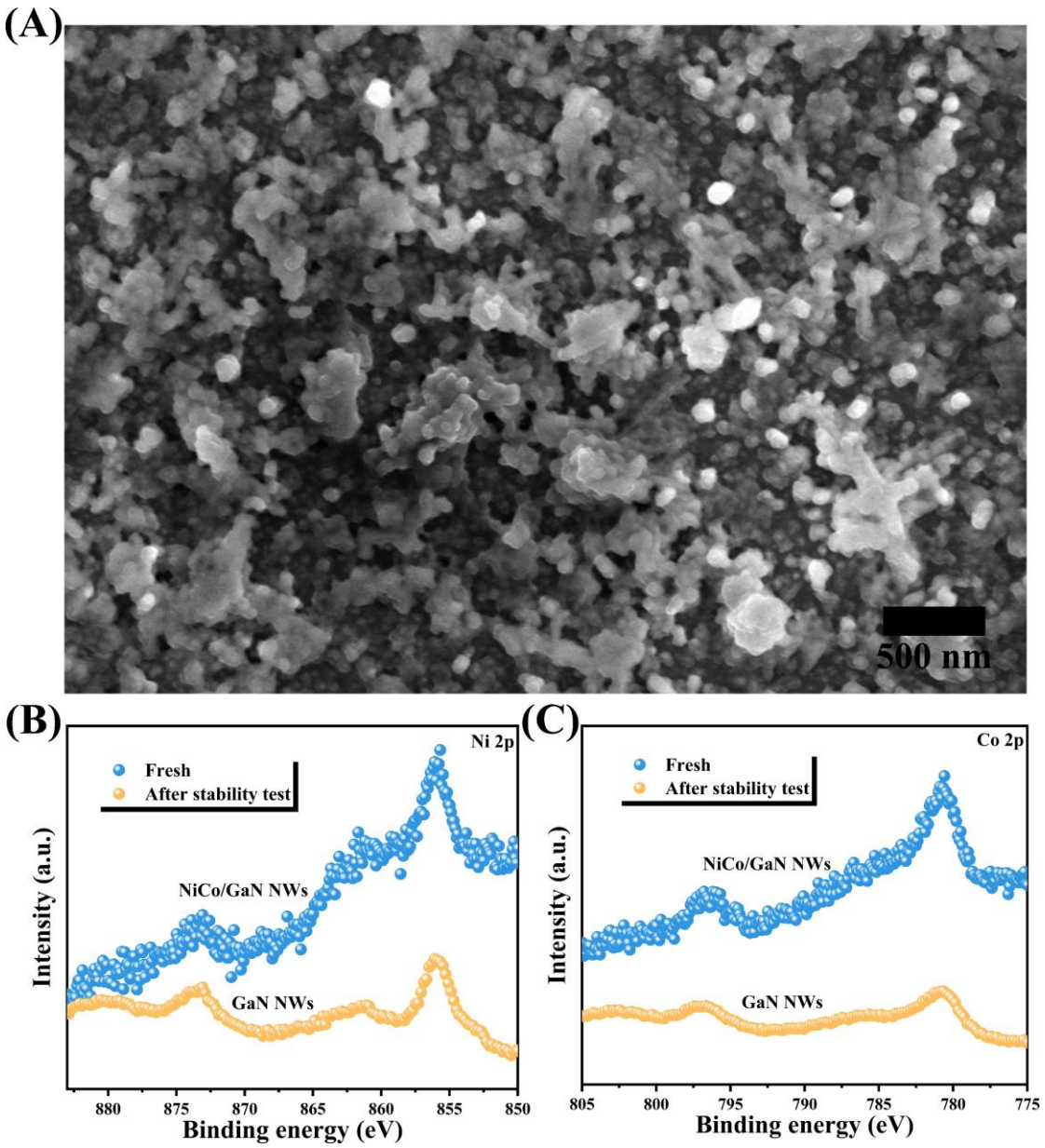


Fig. S14. Characterization of NiCo/GaN NWs after 600 h durability testing. (A) SEM image. HR-XPS of (B) Ni 2p and (C) Co 2p.

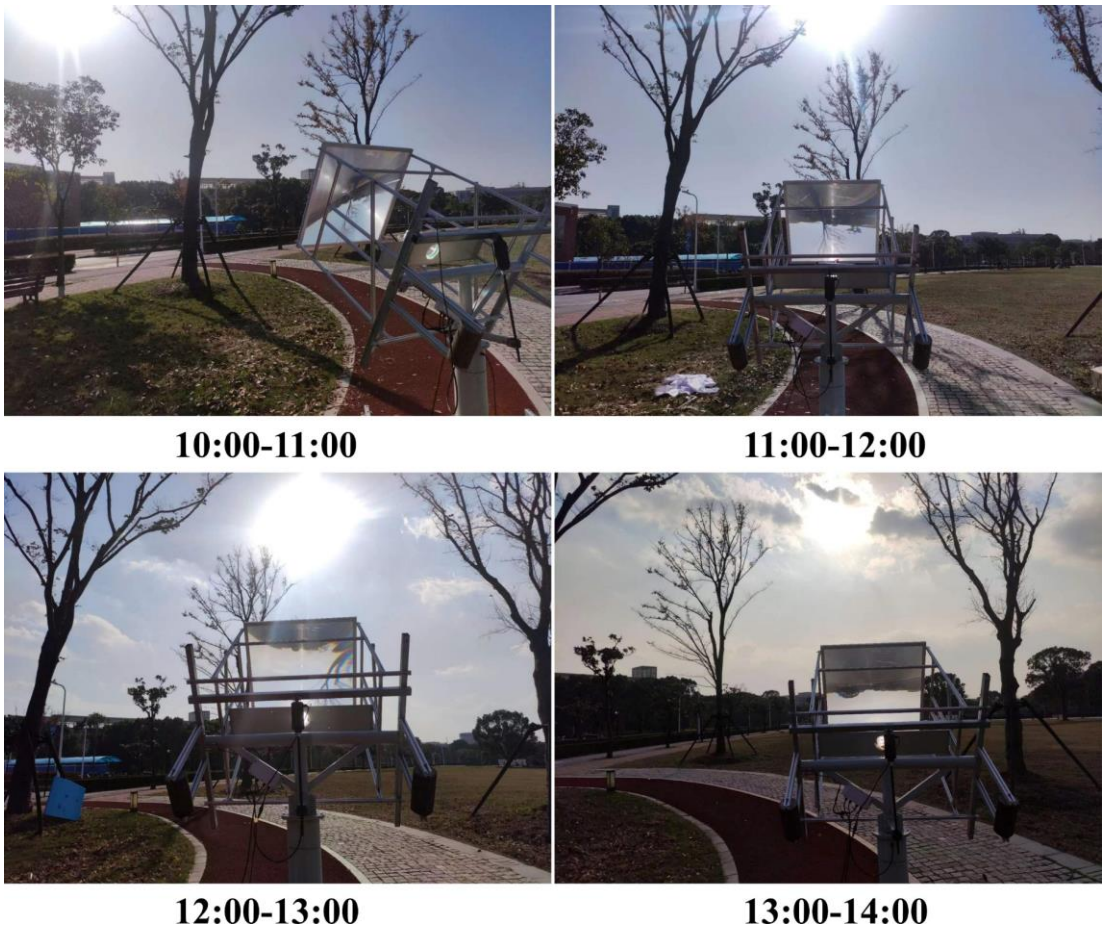


Fig. S15. The photos of the outdoor testing setup equipped with NiCo/GaN NWs supported by silicon wafer at varied testing times recorded at Shanghai Jiao Tong University, Shanghai, P. R. China.

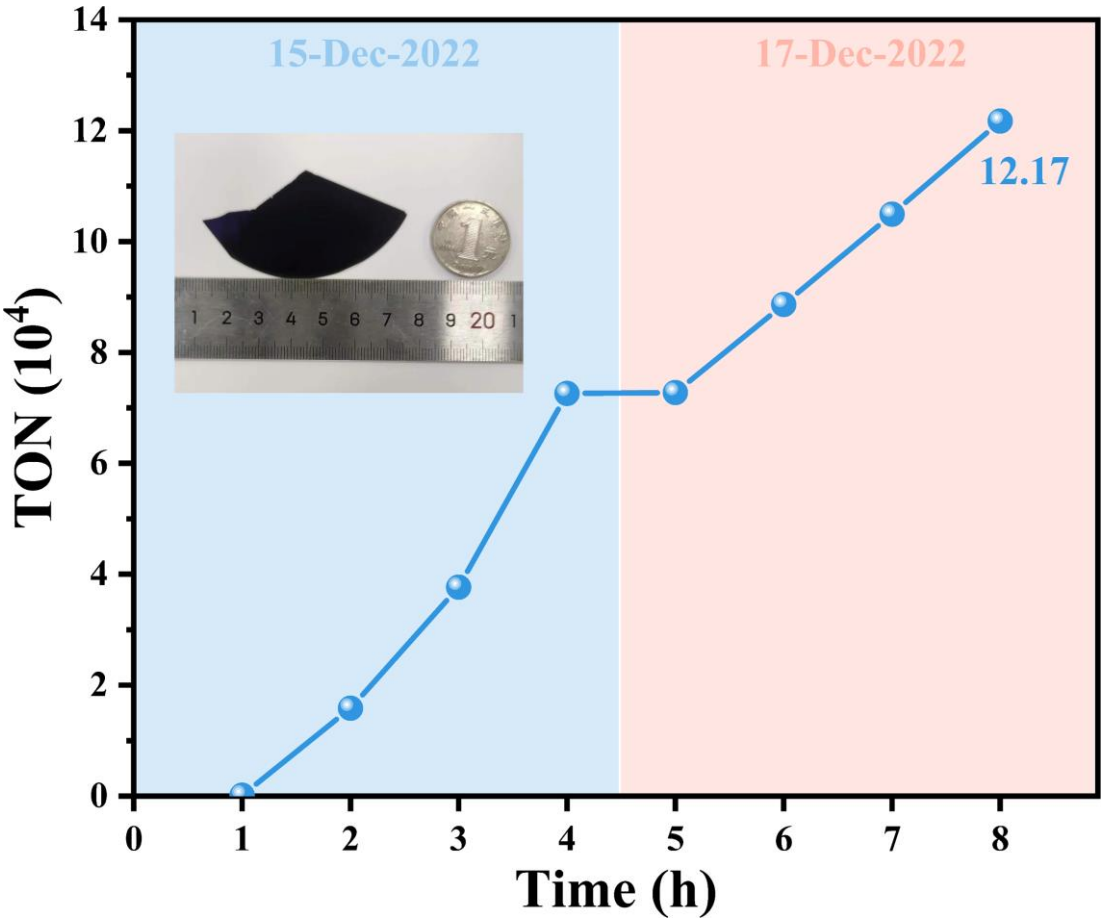


Fig. S16. TON of NiCo/GaN NWs recorded at different times under natural sunlight conditions: 1 W·cm^{-2}~9 W·cm^{-2}. 15-Dec-2022: ambient temperature: 9~11 ℃; air humidity: 41%~53%. 17-Dec-2022: ambient temperature: 3~4 ℃; air humidity: 40%~48%.

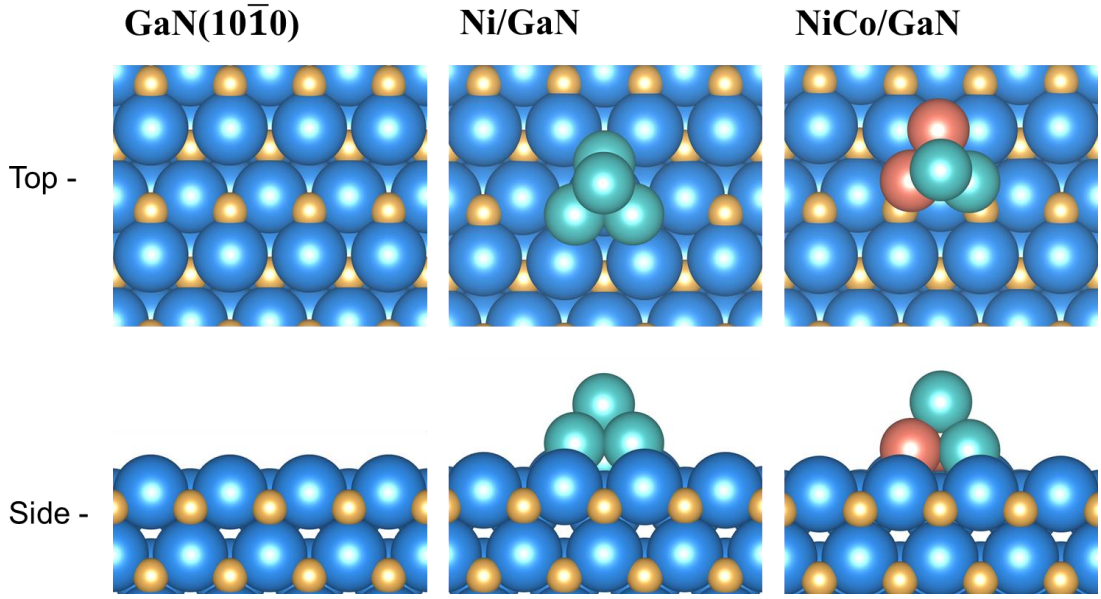


Fig. S17. The top and side views of structural models of GaN ($10\bar{1}0$), Ni/GaN and NiCo/GaN respectively. Ga, blue; N, yellow; Ni, cyan; and Co, orange.

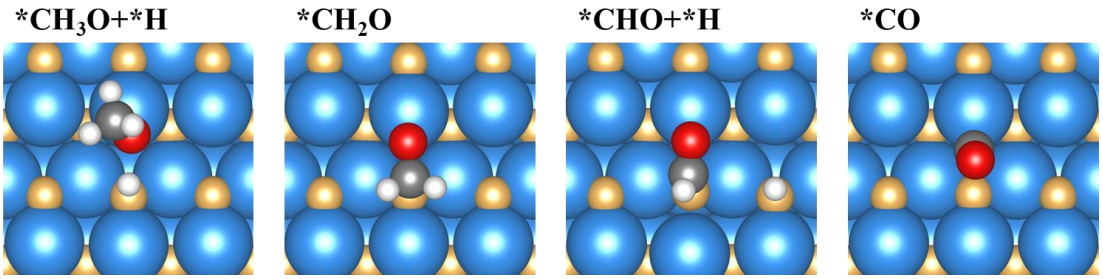


Fig. S18. Optimized adsorption configurations for each reaction intermediates of methanol reforming reaction on GaN ($10\bar{1}0$). Ga, blue; N, yellow; C, grey; O, red; and H, white.

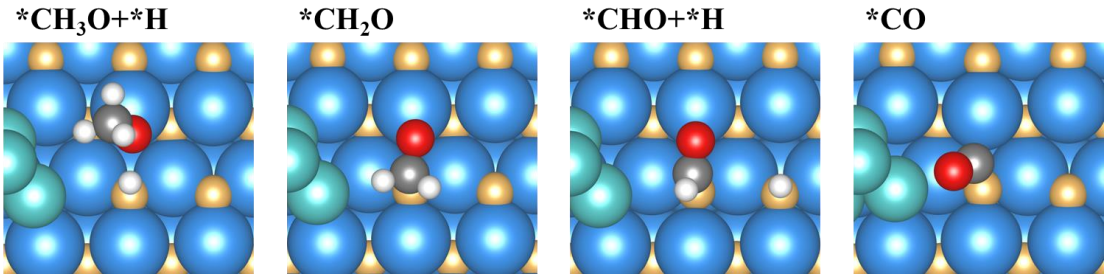


Fig. S19. Optimized adsorption configurations for each reaction intermediates of methanol reforming reaction on Ni/GaN. Ga, blue; N, yellow; Ni, cyan; C, grey; O, red; and H, white.

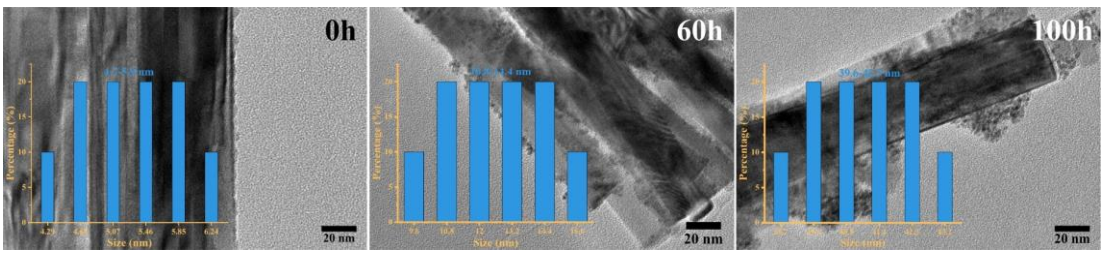


Fig. S20. TEM images and clusters diameters distribution plots of Ni/GaN NWs with various calcinating time (0, 60, and 120 h) at 480 ℃.

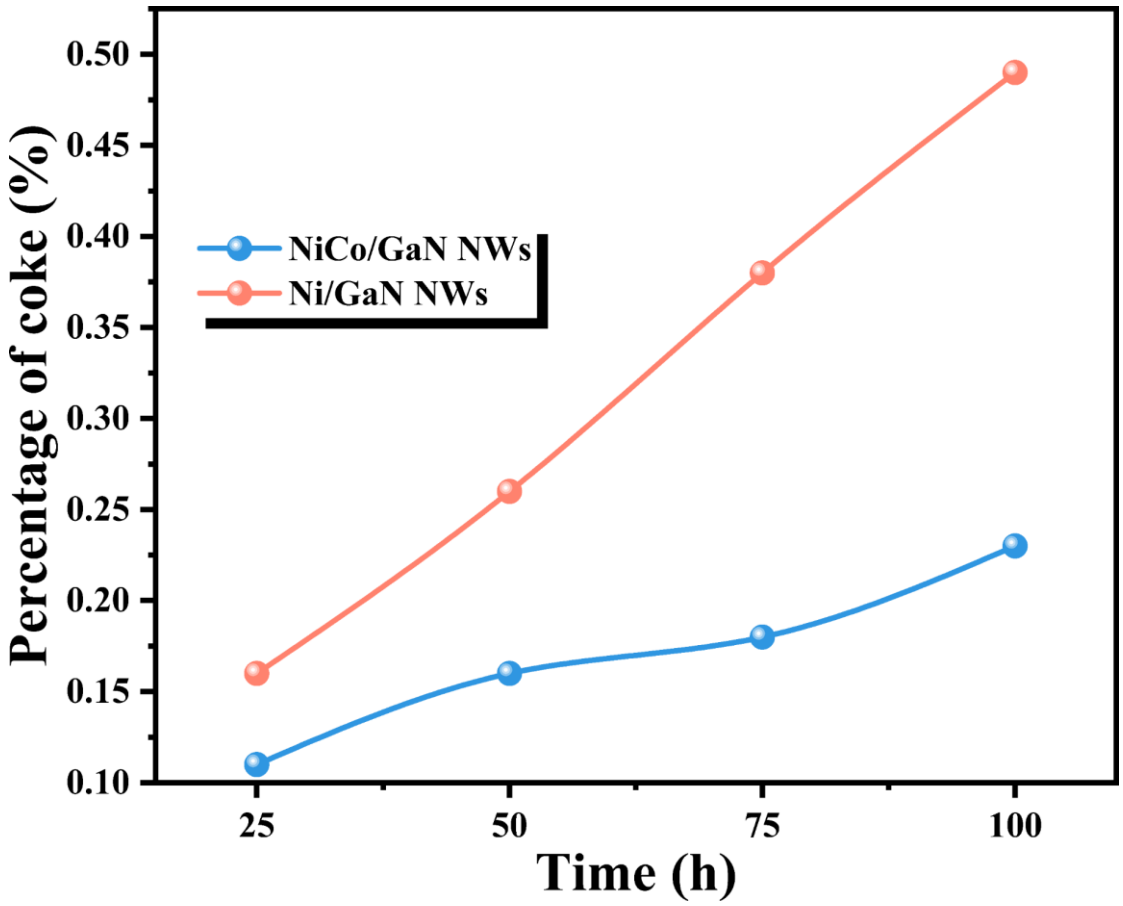


Fig. S21. The coking rate curve is calculated according to **Fig. 4C**.

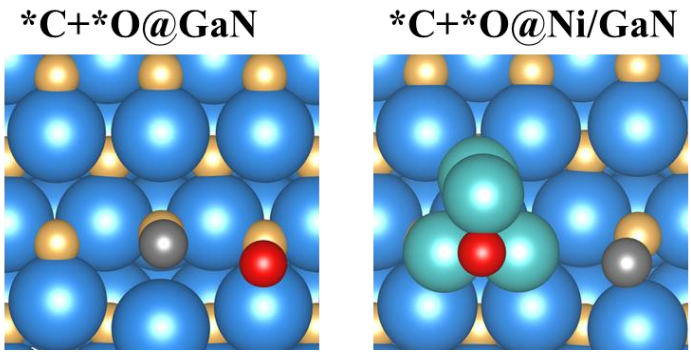


Fig. S22. Optimized adsorption configurations for coke formation on GaN ($10\bar{1}0$) and Ni/GaN. Ga, blue; N, yellow; Ni, cyan; C, grey; and O, red.

References

[1] H. Wang, H. Qi, X. Sun, S. Jia, X. Li, T. J. Miao, L. Xiong, S. Wang, X. Zhang, X. Liu, A. Wang, T. Zhang, W. Huang, J. Tang, *Nat. Mater.* **2023**, 22, 619.

[2] S. Luo, H. Lin, Q. Wang, X. Ren, D. Hernandez-Pinilla, T. Nagao, Y. Xie, G. Yang, S. Li, H. Song, M. Oshikiri, J. Ye, *J. Am. Chem. Soc.* **2021**, 143, 12145.

[3] G. Kresse, D. Joubert, *Phys. Rev. B* **1999**, 59, 1758.

[4] G. Kresse, J. Furthmüller, *Phys. Rev. B* **1996**, 54, 11169.

[5] P. E. Blöchl, *Phys. Rev. B* **1994**, 50, 17953.

[6] J. P. Perdew, K. Burke, M. Ernzerhof, *Phys. Rev. Lett.* **1996**, 77, 3865.

[7] J. P. Perdew, J. A. Chevary, S. H. Vosko, K. A. Jackson, M. R. Pederson, D. J. Singh, C. Fiolhais, *Phys. Rev. B* **1992**, 46, 6671.

[8] S. Grimme, J. Antony, S. Ehrlich, H. Krieg, *J. Chem. Phys.* **2010**, 132, 154104.

[9] S. Grimme, S. Ehrlich, L. Goerigk, *J Comput Chem* **2011**, 32, 1456.

[10] H. J. Monkhorst, J. D. Pack, *Phys. Rev. B* **1976**, 13, 5188.

[11] J. K. Nørskov, J. Rossmeisl, A. Logadottir, L. Lindqvist, J. R. Kitchin, T. Bligaard, H. Jónsson, *J. Phys. Chem. B* **2004**, 108, 17886.

[12] Y. Wang, E. P. Yao, L. Wu, J. Feldmann, J. K. Stolarczyk, *Angew. Chem. Int. Ed.* **2021**, 60, 26694.

[13] S. Fang, Z. Sun, Y. H. Hu, *ACS Catal.* **2019**, 9, 5047.

[14] G. Cui, X. Yang, Y. Zhang, Y. Fan, P. Chen, H. Cui, Y. Liu, X. Shi, Q. Shang, B. Tang, *Angew. Chem. Int. Ed.* **2019**, 58, 1340.